

Adaptive Optics Simulations for Siding Spring

Michael Goodwin^{A,C,D}, Charles Jenkins^{A,E} and Andrew Lambert^B

^A Research School of Astronomy Astrophysics, Australian National University, Mt Stromlo Observatory, via Cotter Rd, Weston, ACT 2611, Australia

^B School of Engineering and Information Technology, UNSW@ADFA

^C Corresponding author. Email: mgoodwin@aao.gov.au

^D Current address: Australian Astronomical Observatory, PO Box 296, Epping, NSW 1710, Australia

^E Current address: Earth Science and Resource Engineering, CSIRO

Abstract:

Using an observational derived model optical turbulence profile (model-OTP) we have investigated the performance of Adaptive Optics (AO) at Siding Spring Observatory (SSO), Australia. The simulations cover the performance for AO techniques of single conjugate adaptive optics (SCAO), multi-conjugate adaptive optics (MCAO) and ground-layer adaptive optics (GLAO). The simulation results presented in this paper predict the performance of these AO techniques as applied to the Australian National University (ANU) 2.3 m and Anglo-Australian Telescope (AAT) 3.9 m telescopes for astronomical wavelength bands J, H and K. The results indicate that AO performance is best for the longer wavelengths (K-band) and in the best seeing conditions (sub 1-arcsecond). The most promising results are found for GLAO simulations (field of view of 180 arcsecs), with the field RMS for encircled energy 50% diameter (EE50d) being uniform and minimally affected by the free-atmosphere turbulence. The GLAO performance is reasonably good over the wavelength bands of J, H and K. The GLAO field mean of EE50d is between 200 mas to 800 mas, which is a noticeable improvement compared to the nominal astronomical seeing (870 to 1700 mas).

Keywords: instrumentation: adaptive optics

1 Introduction

Of interest is the performance of Adaptive Optics (AO) at Siding Spring Observatory (SSO). It could be that the installation of AO for the 2.3 m ANU and 3.9 m AAT may open the door for new science programs and discoveries. Certain AO correction modes may provide encouraging performance gains at SSO, despite the relatively moderate seeing conditions. It is therefore important to ascertain the performance predictions for AO. In addition, AO systems are becoming more achievable and affordable for most astronomical observatories (not the case when adaptive optics was first envisioned by Horace W. Babcock in 1953 (Hardy 1998)). Evidence of this fact is the success of adaptive optics demonstrated with the modern 8-10 m class telescopes. Good performance has been reported with the 10 m Keck II Telescope (van Dam et al. 2006), the 8 m Very Large Telescope (Rousset et al. 2003), the 8.2 m Subaru Telescope (Iye et al. 2004) and 8 m Gemini North Telescope (Stoesz et al. 2004) and others.

To predict the performance of AO at SSO requires the characterisation and modeling of the atmospheric optical turbulence profile (model-OTP) based on observational results. The observational results for turbulence profiling at SSO and model-OTP are reported in the paper 'Characterisation of the Optical Turbulence at Siding Spring' (Goodwin et al. 2012) and in PhD thesis by Goodwin (2009). Adaptive optics simulations use the site-characteristic model of the optical

turbulence profile, or model-OTP, to predict the performance of various adaptive optics technologies.

The purpose of adaptive optics for astronomical telescopes is to remove the wavefront aberrations from the optical path between the science object and the imaging detector. When this is successful the quality of the image is limited by the diffraction limit of the astronomical telescope. Most of the wavefront aberrations are induced by the atmospheric turbulence as random phase perturbations within the beam path. An adaptive optics system attempts to measure these phase perturbations and correct (e.g. spatial phase modulator) them in real-time, typically on timescales of milliseconds, to restore image quality.

Adaptive optics improves the performance of most optical instruments, including spectrographs, interferometers and imaging detectors. Adaptive optics can also compensate for telescope tracking errors and wind buffeting, as well as slow timescale aberrations such as mirror/dome seeing and mirror gravity distortions. Low frequency errors are the largest errors and are controlled by a separate system known as "active optics".

A good introduction the subject of AO can be found in the book 'Adaptive Optics for Astronomical Telescopes' by Hardy (1998). An overview of AO and the various correction modes can be found in the author's PhD thesis titled 'Turbulence profiling at Siding Spring and Las Campanas Observatories' (Goodwin 2009).

This paper discusses the YAO numerical simula-

tion code (authored by Francis Rigaut (Rigaut 2007)) and corresponding performance predictions for the 2.3 m ANU and 3.9 m AAT at SSO. Section 2, 3 and 4 discusses the turbulence model, simulation tool and simulation configurations. Section 5 reports the simulation results. Concluding remarks are provided in section 6.

2 Turbulence Model

The simulation code uses the SSO model-OTP in the paper 'Characterisation of the Optical Turbulence at Siding Spring' Goodwin et al. (2012). The model-OTP is a statistical thin-layer characterization, based on measurements of the turbulence profile above SSO conducted over years 2005 and 2006. The simulation code use fractional layer strengths and are listed in Table 1. The simulation code uses the corresponding layer wind speeds and directions by Goodwin et al. (2012). From Table 1, it is evident that the ground-layer contains the bulk fraction of the turbulence integral. It is noted by Goodwin et al. (2012) and Goodwin (2009) that the free-atmosphere (> 500 m) is comparable to the 'good' seeing astronomical sites, like Cerro Pachon, Chile.

		Model Turbulence Profiles (J , Fractional) - SSO (Run 1-8: May 2005 to June 2006)									
		GL	Good			Typical			Bad		
		FA	Good	Typical	Bad	Good	Typical	Bad	Good	Typical	Bad
Parameter	Units	1	2	3	4	5	6	7	8	9	
37.5	/ 1.0	0.8810	0.7635	0.6139	0.8272	0.7575	0.6564	0.6901	0.6509	0.5897	
250	/ 1.0	0.0464	0.0402	0.0324	0.1294	0.1185	0.1027	0.2815	0.2655	0.2405	
1000	/ 1.0	0.0451	0.0773	0.0870	0.0270	0.0489	0.0592	0.0176	0.0329	0.0417	
3000	/ 1.0	0.0059	0.0708	0.1483	0.0035	0.0447	0.1010	0.0023	0.0301	0.0711	
6000	/ 1.0	0.0038	0.0150	0.0467	0.0023	0.0095	0.0318	0.0015	0.0064	0.0224	
9000	/ 1.0	0.0054	0.0140	0.0289	0.0033	0.0088	0.0197	0.0021	0.0060	0.0139	
13500	/ 1.0	0.0123	0.0192	0.0428	0.0073	0.0122	0.0292	0.0048	0.0082	0.0206	
37.5	m/s	2.1981	2.1981	2.1981	5.6605	5.6605	5.6605	9.4200	9.4200	9.4200	
250	m/s	2.2506	2.2506	2.2506	5.7810	5.7810	5.7810	9.6142	9.6142	9.6142	
1000	m/s	2.5495	6.3707	10.4871	2.5495	6.3707	10.4871	2.5495	6.3707	10.4871	
3000	m/s	5.1620	9.9300	14.7605	5.1620	9.9300	14.7605	5.1620	9.9300	14.7605	
6000	m/s	19.0935	23.4552	27.9741	19.0935	23.4552	27.9741	19.0935	23.4552	27.9741	
9000	m/s	32.0000	38.6276	43.7936	32.0000	38.6276	43.7936	32.0000	38.6276	43.7936	
13500	m/s	10.4619	26.4419	41.6250	10.4619	26.4419	41.6250	10.4619	26.4419	41.6250	
J_{GL}	$10^{-13}m^{1/3}$	4.9614	4.9614	4.9614	8.5562	8.5562	8.5562	13.2849	13.2849	13.2849	
J_{FA}	$10^{-13}m^{1/3}$	0.3880	1.2115	2.7159	0.3880	1.2115	2.7159	0.3880	1.2115	2.7159	
J	$10^{-13}m^{1/3}$	5.3493	6.1729	7.6773	8.9442	9.7678	11.2721	13.6728	14.4964	16.0008	
F_{GL}	/ 1.0	0.9275	0.8037	0.6462	0.9566	0.8760	0.7591	0.9716	0.9164	0.8303	
F_{FA}	/ 1.0	0.0725	0.1963	0.3538	0.0434	0.1240	0.2409	0.0284	0.0836	0.1697	
ϵ_{GL}	arcsecs	0.8277	0.8277	0.8277	1.1478	1.1478	1.1478	1.4945	1.4945	1.4945	
ϵ_{FA}	arcsecs	0.1794	0.3552	0.5766	0.1794	0.3552	0.5766	0.1794	0.3552	0.5766	
ϵ	arcsecs	0.8659	0.9436	1.0755	1.1787	1.2427	1.3542	1.5206	1.5749	1.6710	
θ_0	arcsecs	6.4233	3.7172	2.0123	6.3684	3.7043	2.0098	6.2255	3.6700	2.0030	
τ	ms	11.7922	5.3516	2.3291	4.5855	3.5038	2.0310	2.2067	2.0112	1.5242	
Probability	/ 1.0	0.0625	0.1250	0.0625	0.1250	0.2500	0.1250	0.0625	0.1250	0.0625	

Table 1 Tabulated values for the final model-OTP for the SSO (Run 1-8: May 2005 to June 2006), with layers specified as fractional amount of total turbulence integral, J , with corresponding wind speed, m/s (Goodwin et al. 2012; Goodwin 2009).

3 Simulation Code

The simulation code used to perform the adaptive simulations is an open source numerical simulation code called YAO, written by Francis Rigaut (Rigaut 2007). The YAO simulation code is a Monte-Carlo adaptive optics simulation tool coded in YORICK (Munro 2005). YORICK is an open source interpreted programming language for scientific simulation codes. The YAO simulation code has custom developed functions to simulate the wavefront sensor (WFS), the deformable mirror (DM) and other aspects of an adaptive optics loop (Rigaut 2007). The YAO simulation code is provided with a set of example scripts which can be easily modified to simulate SCAO, MCAO and GLAO for a specific model atmosphere, telescope and adaptive optics system configuration. The YAO simulation code was selected based on its extensive functionality, ease of use (documentation and examples), as well as being open source software. The YAO simulation code has been verified with independent code for the case of SCAO (Goodwin 2009).

mags for tip-tilt sensing seems appropriate as performance starts to fall-off with fainter tip-tilt stars.

Table 2 Estimated sky coverage for SCAO based on NGS (tip-tilt) search radius of 30" from LGS (science target).

Tilt NGS m_R	15	17	19
Galactic Latitude 30	12%	35%	73%
Galactic Latitude 90	4%	12%	28%

4 Simulation Configurations

The simulation results are based on the adaptive optics correction modes of SCAO, MCAO and GLAO for the ANU 2.3 m and AAT 3.9 m using the YAO adaptive optics numerical simulation code. Each adaptive optics correction mode and telescope specification is associated with a set of simulation input configuration parameters and system geometry.

The schematic for the system geometry of the SCAO, MCAO and GLAO adaptive optics models as used with the ANU 2.3 m and AAT 3.9 m telescopes are shown in Figure 1. The large number of field stars (FS) in Figure 1 (b) and (c) are artificial and inserted onto a regular grid to calculate the Strehl, FWHM and EE50d performance parameters as a function of field location.

The input configuration parameters for the SCAO adaptive optics model as used with the ANU 2.3 m and AAT 3.9 m telescopes are tabulated in Table 3. The sky coverage for the SCAO adaptive optics model, given a NGS (tip-tilt) magnitude within a search radius of 30" from LGS (science target), as used with the ANU 2.3 m and AAT 3.9 m telescopes, is tabulated in Table 2, and were calculated by Chun et al. (2000).

The input configuration parameters for the MCAO adaptive optics model as used with the ANU 2.3 m and AAT 3.9 m are tabulated in Table 4.

The input configuration parameters for the GLAO adaptive optics model as used with the ANU 2.3 m and AAT 3.9 m are tabulated in Table 5.

The input parameters, e.g. mirror type and transmission, were in part adapted from the test examples that were distributed with YAO given the complexity involved in the simulations. The hardware simulation choices are based on readily available technology at the time of simulation (around the year 2008/2009). The parameters were sensible and kept consistent amongst the correction modes, e.g. for SCAO, a NGS of 15

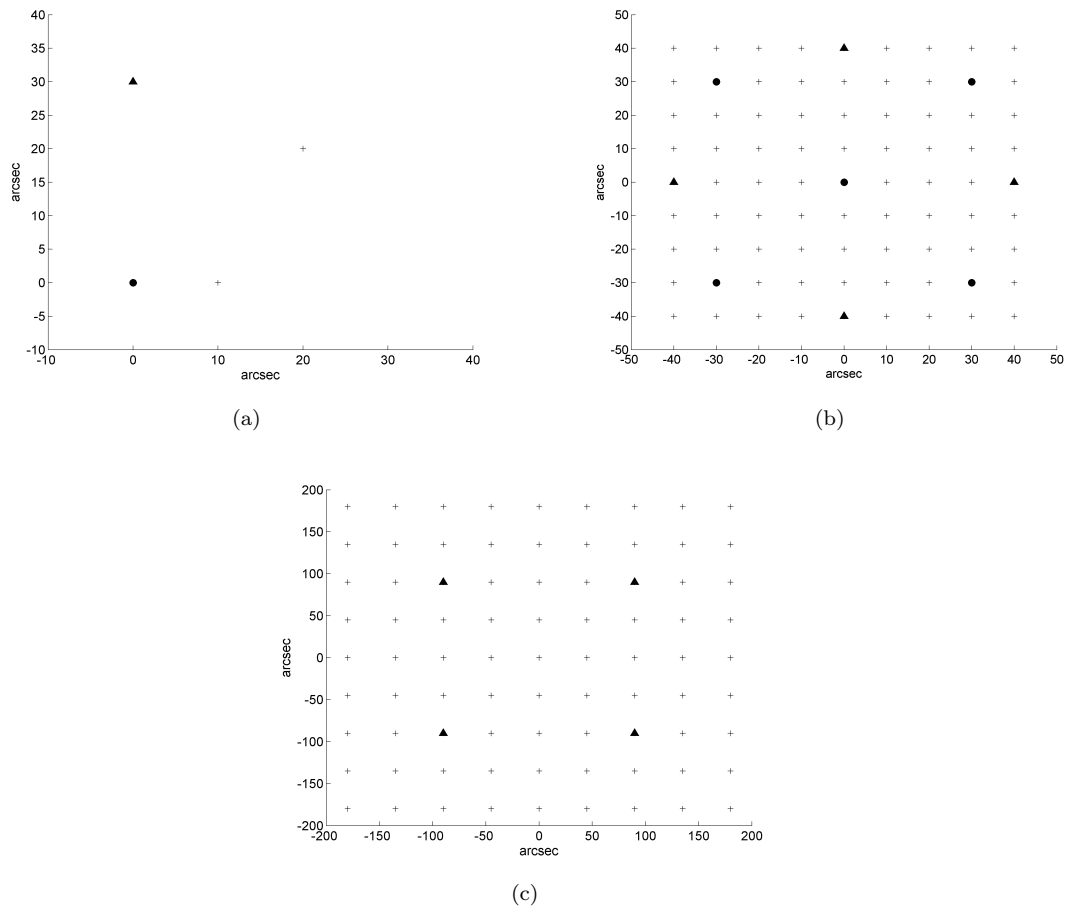


Figure 1 Geometry of configurations for (a) SCAO (b) MCAO and (c) GLAO configurations as used in adaptive optics simulations for the ANU 2.3 m and AAT 3.9 m telescopes. The NGS are marked with filled triangles; LGS are marked with filled circles and Field stars (FS) as plus signs.

Table 3. Parameters of the models used in SCAO simulation codes.

Parameter (SCAO)	ANU 2.3m	AAO 3.9m
Model-OTP	SSO	SSO
LGS (high order source)		
LGS Position (x,y)	(0",0")	(0",0")
LGS Power	10W	10W
LGS Sodium Layer Altitude	95,000m	95,000m
LGS Sodium Layer Thickness	8,000m	8,000m
LGS Return (photons/cm ² /s/W)	30	30
NGS (tip/tilt source)		
NGS Position (x,y)	(0",30")	(0",30")
NGS mR	15 (17,19)	15 (17,19)
WFS (high order sensing)	LGS	LGS
WFS (Shack Hartmann)	11x11	14x14
WFS Subaperture (Pixels)	8x8	8x8
WFS Pixel Scale	0.5" / pixel	0.5" / pixel
WFS Read Noise RMS (e/pixel)	2	2
WFS Frame Rate	500 fps	500 fps
WFS Wavelength	589nm	589nm
WFS (tip/tilt sensing)	NGS	NGS
WFS (Shack Hartmann, APD)	1x1	1x1
WFS Subaperture (Pixels)	4x4	4x4
WFS Pixel Scale	0.5" / pixel	0.5" / pixel
WFS Read Noise RMS (e/pixel)	0	0
WFS Frame Rate	50 fps	50 fps
WFS Wavelength	700nm	700nm
DM Conjugate Height	0m	0m
DM Actuators (DOF)	113	177
Field Stars		
FS 1 Position (x,y)	(0",0")	(0",0")
FS 2 Position (x,y)	(0",10")	(0",10")
FS 3 Position (x,y)	(20",20")	(20",20")
FS Wavelengths (microns)	1.2, 1.65, 2.2	1.2, 1.65, 2.2
FS Integration Time	2s	2s
FS Zenith Angle	0	0

Table 4. Parameters of the models used in MCAO simulation code.

Parameter (MCAO)	ANU 2.3m	AAO 3.9m
Model-OTP	SSO	SSO
LGS (high order source)		
LGS 1 Position (x,y)	(-30",-30")	(-30",-30")
LGS 2 Position (x,y)	(30",-30")	(30",-30")
LGS 3 Position (x,y)	(0",0")	(0",0")
LGS 4 Position (x,y)	(-30",30")	(-30",30")
LGS 5 Position (x,y)	(30",30")	(30",30")
LGS Power	10W	10W
LGS Sodium Layer Altitude	95,000m	95,000m
LGS Sodium Layer Thickness	8,000m	8,000m
LGS Return (photons/cm ² /s/W)	30	30
NGS (tip/tilt source)		
NGS 1 Position (x,y)	(40",0")	(40",0")
NGS 2 Position (x,y)	(0",-40")	(0",-40")
NGS 3 Position (x,y)	(-40",0")	(-40",0")
NGS 4 Position (x,y)	(0",40")	(0",40")
NGS mR	5	5
WFS (high order sensing)	LGS	LGS
WFS (Shack Hartmann)	11x11	14x14
WFS Subaperture (Pixels)	4x4	4x4
WFS Pixel Scale	0.5" / pixel	0.5" / pixel
WFS Read Noise RMS (e/pixel)	2	2
WFS Frame Rate	500 fps	500 fps
WFS Wavelength	589nm	589nm
WFS (tip/tilt sensing)	NGS	NGS
WFS (Shack Hartmann, APD)	1x1	1x1
WFS Subaperture (Pixels)	4x4	4x4
WFS Pixel Scale	0.5" / pixel	0.5" / pixel
WFS Read Noise RMS (e/pixel)	0	0
WFS Frame Rate	50 fps	50 fps
WFS Wavelength	700nm	700nm
DM 1 Conjugate Height	0m	0m
DM 1 Actuators (DOF)	113	177
DM 2 Conjugate Height	2000m	2000m
DM 2 Actuators (DOF)	201	380
DM 3 Conjugate Height	7000m	7000m
DM 3 Actuators (DOF)	79	201
Field Stars		
FS Position (x,y)		
(0",0")- (40",40")	5x5 grid	5x5 grid
FS Wavelengths (microns)	1.2, 1.65, 2.2	1.2, 1.65, 2.2
FS Integration Time	1s	1s
FS Zenith Angle	0	0

Table 5. Parameters of the models used in GLAO simulation code.

Parameter (GLAO)	ANU 2.3m	AAO 3.9m
NGS (high order, tip/tilt source)		
NGS 1 Position (x,y)	(90",90")	(90",90")
NGS 2 Position (x,y)	(90",-90")	(90",-90")
NGS 3 Position (x,y)	(-90",-90")	(-90",-90")
NGS 4 Position (x,y)	(-90",90")	(-90",90")
NGS mR	11	11
WFS (high order sensing)	NGS	NGS
WFS (Shack Hartmann)	11x11	18x18
WFS Subaperture (Pixels)	4x4	4x4
WFS Pixel Scale	0.75" / pixel	0.5" / pixel
WFS Read Noise RMS (e/pixel)	2	2
WFS Frame Rate	200 fps	200 fps
WFS Wavelength	700nm	700nm
DM Conjugate Height	0m	0m
DM Type	Bimorph	Bimorph
Field Stars		
FS Position (x,y)		
(-180", -180")- (180",180")	9x9 grid	9x9 grid
FS Wavelengths (microns)	1.2, 1.65, 2.2	1.2, 1.65, 2.2
FS Integration Time	1.25s	1.25s
FS Zenith Angle	0	0

5 Simulation Results

This section reports the results of adaptive optics techniques SCAO, MCAO and GLAO as applied to the ANU 2.3 m and AAT 3.9 m telescopes for wavelength bands J, H and K using the SSO model-OTP as tabulated in Table 1, see §2.

5.1 SCAO Results

The input SCAO configuration parameters as used in the YAO simulation code for the ANU 2.3 m are tabulated in Table 3 with a schematic of the geometry shown in Figure 1. Likewise for the AAT 3.9 m the parameters are tabulated in Table 3 and the geometry shown in Figure 1.

To model the sky coverage performance, the Strehl results are shown in Figure 2 (ANU 2.3 m) and Figure 3 (AAT 3.9 m) for three tip-tilt NGS of increasing limiting magnitude, m_R . The percentage of sky coverage for these tip-tilt NGS are tabulated in Table 2. From Figure 2 and Figure 3 it can be seen that both telescopes have similar trends in Strehl performance for model atmospheres 1-9. However, the AAT 3.9 m shows a marginally poorer performance in Strehl. A noticeable drop in Strehl occurs for a tilt guide star magnitude $m_R = 19$ (73% sky coverage at 30 degrees galactic latitude) for all model atmospheres. This is unacceptable performance, particularly for the shortest wavelength J-band. It is also noted that the H-band and K-band have poor Strehls for model atmospheres 7-9 that represent a bad ground-layer resulting in the worst overall seeing conditions. Noticeable improvements the Strehl occur for H-band and K-band for model atmospheres 1 and 4, both having good free-atmosphere conditions with a good/typical ground layer.

To model the anisoplanatism (correction field of view) performance the Strehl results are shown in Figure 4 (ANU 2.3 m) and Figure 5 (AAT 3.9 m) for three field stars of increasing angular distance from LGS (science target). From Figure 4 and Figure 5 we note similar trends in performance of both telescopes. The Strehl decreases gradually, but almost identical, for increasing angular distance of the field stars. The Strehl increases for the longer wavelengths, with highest values for the K-band. Noticeable improvements the Strehl occur for model atmospheres 1 and 4 (good free-atmosphere conditions). The results indicate that relatively large correction fields of view are possible, $\sim 30''$.

5.2 MCAO Results

The input MCAO configuration parameters as used in the YAO simulation code for the ANU 2.3 m and AAT 3.9 m are tabulated in Table 4 with a schematic of the geometry shown in Figure 1. The EE50d parameter (units of milli-arcseconds) is used as the figure of merit to assess the performance of the MCAO simulations. A representative contour plot of the EE50d over the designed angular field of view for the AAT 3.9 m telescope with the SSO Model-OTP (1-9) for H-band

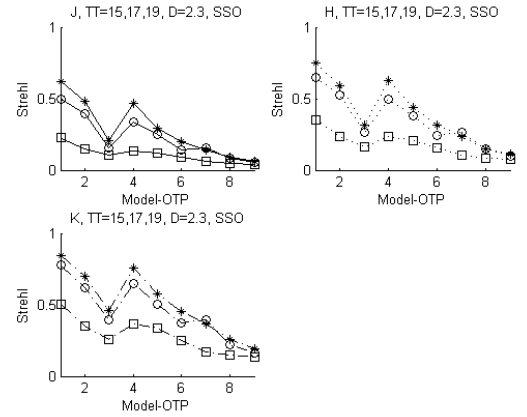


Figure 2 YAO numerical SCAO simulation Strehl results for tilt guide star having $m_R=15$ (asterisks), 17 (open circles), 19 (open squares) for the ANU 2.3m telescope with the SSO Model-OTP (1-9). This simulation models sky coverage performance for wavelength bands J, H and K.

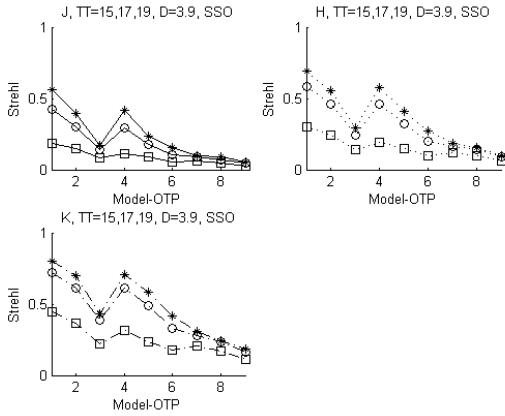


Figure 3 YAO numerical SCAO simulation Strehl results for tilt guide star having $m_R=15$ (asterisks), 17 (open circles), 19 (open squares) for the AAT 3.9 m telescope with the SSO Model-OTP (1-9). This simulation models sky coverage performance.

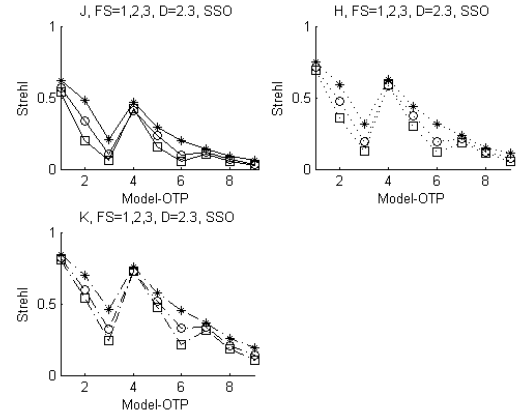


Figure 4 YAO numerical SCAO simulation Strehl results for field stars having $m_R=15$ and angular distance from LGS (x,y) in arcsecs of (0,0) (asterisks), (0,10) (open circles), (20,20) (open squares) for the ANU 2.3 m telescope with the SSO Model-OTP (1-9). This simulation models anisoplanatism (correction FOV) performance for wavelength bands J, H and K.

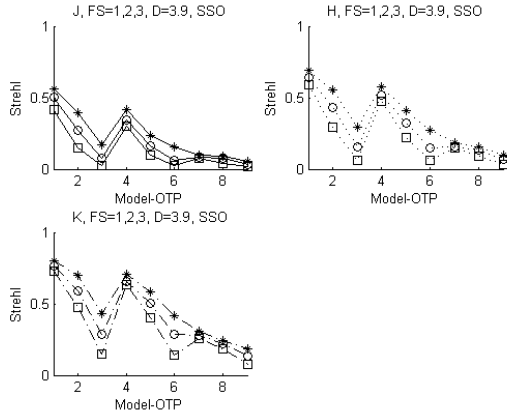


Figure 5 YAO numerical SCAO simulation Strehl results for field stars having $m_R=15$ and angular distance from LGS (x,y) in arcsecs of (0,0) (asterisks), (0,10) (open circles), (20,20) (open squares) for the AAT 3.9 m telescope with the SSO Model-OTP (1-9). This simulation models anisoplanatism (correction FOV) performance.

is shown in Figure 10. The nominal correction field of view for MCAO simulations is 80 arcseconds. A summary of MCAO simulation results for EE50d parameter's field mean and field RMS for the ANU 2.3 m and AAT 3.9 m are shown in Figure 6 and Figure 7.

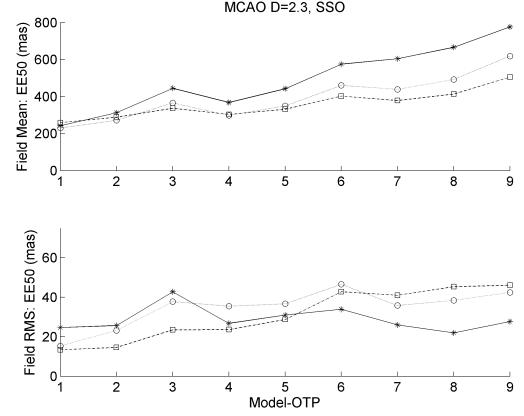


Figure 6 MCAO simulation results summary (using YAO) for EE50d parameter (units of milli-arcseconds) for field mean and field RMS at J-Band (asterisks), H-band (open circles), K-band (open squares) wavelengths for the ANU 2.3 m telescope with the SSO Model-OTP (1-9).

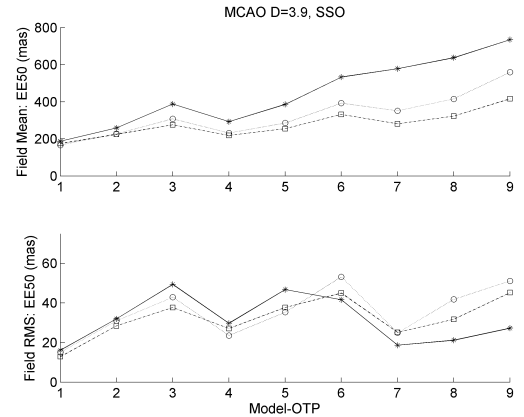


Figure 7 MCAO simulation results summary (using YAO) for EE50d parameter (units of milli-arcseconds) for field mean and field RMS at J-Band (asterisks), H-band (open circles), K-band (open squares) wavelengths for the AAT 3.9 m telescope with the SSO Model-OTP (1-9).

From Figure 6 and Figure 7 we note similar trends in MCAO performance of both telescopes. The results for MCAO simulations for SSO having FOV of 80 arcsecs, show sensitivity to the ground-layer turbulence with the poorest EE50d results for 'bad' ground-layer conditions (poorest seeing), particularly for the shortest wavelength, or J-band. Reasonable MCAO results

for SSO are achievable for longer wavelengths of H-band and K-band, with field mean of EE50d between 200 to 400 mas and corresponding field RMS between 20 to 50 mas. Conditions of strong free-atmosphere turbulence (model atmospheres 3, 6 and 9) increases both the mean and RMS of EE50d, but the MCAO sensitivity to the free-atmosphere is somewhat less than that for the SCAO performances. The EE50d contour plot shown in Figure 10 for bad free-atmosphere conditions show the best corrections around the placement of the 5 LGS (hence large field RMS of EE50d).

5.3 GLAO Results

The input GLAO configuration parameters as used in the YAO simulation code for the ANU 2.3 m and the AAT 3.9 m are tabulated in Table 5 with a schematic of the geometry shown in Figure 1. The EE50d parameter (units of milli-arcseconds) is used as the figure merit to assess the performance of the GLAO simulations. A representative contour plots of the EE50d over the designed angular field of view for the AAT 3.9 m telescope with the SSO Model-OTP (1-9) have been simulated for wavelength H-band (Figure 11). The nominal correction field of view is 180 arcseconds. A summary of GLAO simulation results for EE50d parameter's field mean and field RMS for ANU 2.3 m and AAT 3.9 m are shown in Figure 8 and Figure 9.

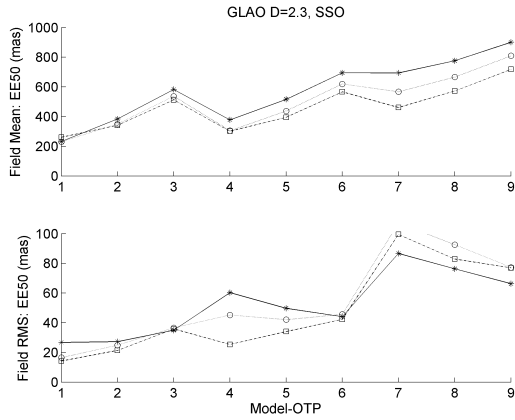


Figure 8 GLAO simulation results summary (using YAO) for EE50d parameter (units of milli-arcseconds) for field mean and field RMS at J-Band (asterisks), H-band (open circles), K-band (open squares) wavelengths for the ANU 2.3 m telescope with the SSO Model-OTP (1-9).

From Figure 8 and Figure 9 we note similar trends in GLAO performance of both telescopes, except that the AAT 3.9 m has a lower, more uniform field RMS for EE50d. The results of GLAO also shows a performance trend that is similar to MCAO. Performance becomes poorer at shorter wavelengths and bad free-atmosphere conditions, with field mean of EE50d between 200 to 800 mas and corresponding field RMS between 20 to 100 mas for all model atmospheres.

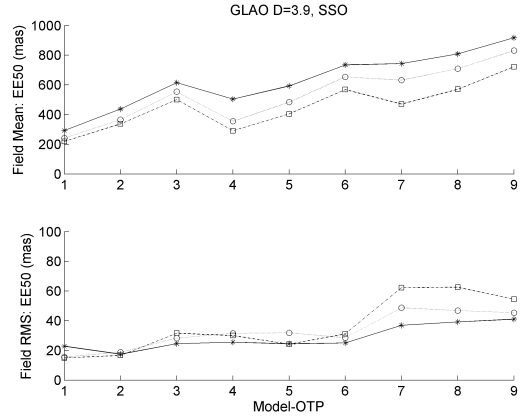


Figure 9 GLAO simulation results summary (using YAO) for EE50 parameter (units of milli-arcseconds) for field mean and field RMS at J-Band (asterisks), H-band (open circles), K-band (open squares) wavelengths for the AAT 3.9 m telescope with the SSO Model-OTP (1-9).

The relatively good results from the GLAO simulations may need caution due to the coarse sampling of the ground layer (37.5m, 250m and 1000m) may be insufficient to accurately model the behaviour of a 3' FoV system. The coarse sampling can lead to obtaining a GLAO result that is too optimistic. A test to split the first few layers into many would help to verify that sampling is sufficient. This could not be fully explored due to simulation time constraints (more layers increase simulations times) and that the model is kept constant for consistent comparison of adaptive optic correction modes.

6 Conclusions

This paper has reported on our adaptive optic simulations for ANU 2.3 m and AAT 3.9 m telescopes based on the YAO simulation code. A summary of results has been presented for SCAO, MCAO and GLAO based on a model-OTP derived from measurements at SSO spanning years 2005 to 2006. The results indicate that adaptive optics performance is best for the longer wavelengths (K-band) and in the best seeing conditions (sub 1-arcsecond).

The results for SCAO simulations for SSO show sensitivity in performance to the turbulence strength in the free-atmosphere. For a 'good' free-atmosphere the Strehl is excellent while for a 'bad' free-atmosphere the Strehl is dismal. A decreasing trend in performance is also observed for an increasing ground-layer strength (poorer seeing). Results suggest anisoplanatism (distance of tip-tilt NGS from science target) has a minimal impact for FOV. Performance improves for longer wavelengths with the best performance in the K-band. Note that the SCAO results for SSO use a powerful 10 W sodium LGS (comparable to Altair LGS for Gemini-N). The reason being that the sub-

aperture sizes are smaller at SSO due to the relatively poor seeing and hence more photons are needed for wavefront sensing. We believe it to be technically feasible for SSO to implement SCAO but it would be an expensive project due to the 10 W sodium LGS. The operation of SCAO for SSO (for Strehls between 0.3 to 0.8) would be limited to larger wavelengths (e.g., K-band) with sky coverage of $\sim 35\%$ (galactic latitude of 30 degrees) for $\sim 50\%$ of nights having suitable conditions.

The results for MCAO simulations for SSO having FOV of 80 arcsecs, show sensitivity to the ground-layer turbulence with the poorest EE50d results for 'bad' ground-layer conditions (poorest seeing), particularly for the shortest wavelength, or J-band. Conditions of strong free-atmosphere turbulence increases the field RMS of EE50d and hence would be unsuitable for some astronomical science cases. The cost and complexity of MCAO is significantly higher than SCAO due to the requirement of multiple LGS and NGS with associated WFS and DM. Therefore, we do not recommend MCAO as a viable option for SSO.

The results for GLAO simulations for SSO having FOV of 180 arcsec, show a similar trend and performance to that of the MCAO results. However, the GLAO field RMS for EE50d is more uniform and minimally affected by the free-atmosphere turbulence for the AAT 3.9 m. The performance is reasonably good over the wavelength bands of J, H and K. The field mean of EE50d is between 200 mas to 800 mas, which is a noticeable improvement compared to the nominal astronomical seeing (870 to 1700 mas). GLAO has the advantage of performing active optics (static and gravity / temperature variations) and also correcting for dome seeing. GLAO is also well suited to use Rayleigh LGS that are cheaper with 'industry strength' lasers commercially available. The implementation of GLAO for SSO is therefore technically feasible given the technical requirements of multiple NGSs (or Rayleigh LGS) over a large field radius. Therefore, we recommend GLAO as a promising option for SSO.

Acknowledgments

This work makes use of observational data and analysis provided by the author's PhD thesis research conducted at the Research School of Astronomy and Astrophysics (RSAA) of the Australian National University (ANU). The authors are grateful to Jon Lawrence of the Australian Astronomical Observatory (AAO) for his suggestions for the original version of the manuscript and to the referees for their comments.

References

- Chun, M. R., D'Orgeville, C., Ellerbroek, B. L., Graves, J. E., Northcott, M. J., and Rigaut, F. J.: 2000, in P. L. Wizinowich (ed.), *Society of Photo-Optical Instrumentation Engineers (SPIE) Conference Series*, Vol. 4007 of *Society of Photo-Optical Instrumentation Engineers (SPIE) Conference Series*, pp 142–148
- Goodwin, M.: 2009, *Turbulence profiling at Siding Spring and Las Campanas Observatories*, ANU PhD Thesis
- Goodwin, M., Jenkins, J., and Lambert, A.: 2012, *Characterisation of the Optical Turbulence at Siding Spring (accepted to appear in PASA)*
- Hardy, J. W.: 1998, *Adaptive Optics for Astronomical Telescopes*, Adaptive Optics for Astronomical Telescopes, by John W Hardy, pp. 448. Foreword by John W Hardy. Oxford University Press, Jul 1998. ISBN-10: 0195090195. ISBN-13: 9780195090192
- Iye, M., Takami, H., Takato, N., Oya, S., Hayano, Y., Guyon, O., Colley, S. A., Hattori, M., Watanabe, M., Eldred, M., Saito, Y., Saito, N., Akagawa, K., and Wada, S.: 2004, in W. Jiang and Y. Suzuki (eds.), *Adaptive Optics and Applications III. Edited by Jiang, Wenhan; Suzuki, Yoshiji. Proceedings of the SPIE, Volume 5639, pp. 1-10 (2004).*, Vol. 5639 of *Presented at the Society of Photo-Optical Instrumentation Engineers (SPIE) Conference*, pp 1–10
- Munro, D. H.: 2005, *Yorick: Interpreted programming language v2.1.05*, <http://yorick.sourceforge.net/>
- Rigaut, F.: 2007, *Yao: An adaptive optics simulation tool v4.2.3*, <http://www.maumae.net/yao/aosimul.html>
- Rousset, G., Lacombe, F., Puget, P., Hubin, N. N., Gendron, E., Fusco, T., Arsenault, R., Charton, J., Feautrier, P., Gigan, P., Kern, P. Y., Lagrange, A.-M., Madec, P.-Y., Mouillet, D., Rabaud, D., Rabou, P., Stadler, E., and Zins, G.: 2003, in P. L. Wizinowich and D. Bonaccini (eds.), *Adaptive Optical System Technologies II. Edited by Wizinowich, Peter L.; Bonaccini, Domenico. Proceedings of the SPIE, Volume 4839, pp. 140-149 (2003).*, Vol. 4839 of *Presented at the Society of Photo-Optical Instrumentation Engineers (SPIE) Conference*, pp 140–149
- Stoesz, J. A., Veran, J.-P., Rigaut, F. J., Herriot, G., Jolissaint, L., Frenette, D., Dunn, J., and Smith, M.: 2004, in D. Bonaccini Calia, B. L. Ellerbroek, and R. Ragazzoni (eds.), *Advancements in Adaptive Optics. Edited by Domenico B. Calia, Brent L. Ellerbroek, and Roberto Ragazzoni. Proceedings of the SPIE, Volume 5490, pp. 67-78 (2004).*, Vol. 5490 of *Presented at the Society of Photo-Optical Instrumentation Engineers (SPIE) Conference*, pp 67–78
- van Dam, M. A., Bouchez, A. H., Le Mignant, D., Johansson, E. M., Wizinowich, P. L., Campbell, R. D., Chin, J. C. Y., Hartman, S. K., Lafon, R. E., Stomski, Jr., P. J., and Summers, D. M.: 2006, *PASP* **118**, 310

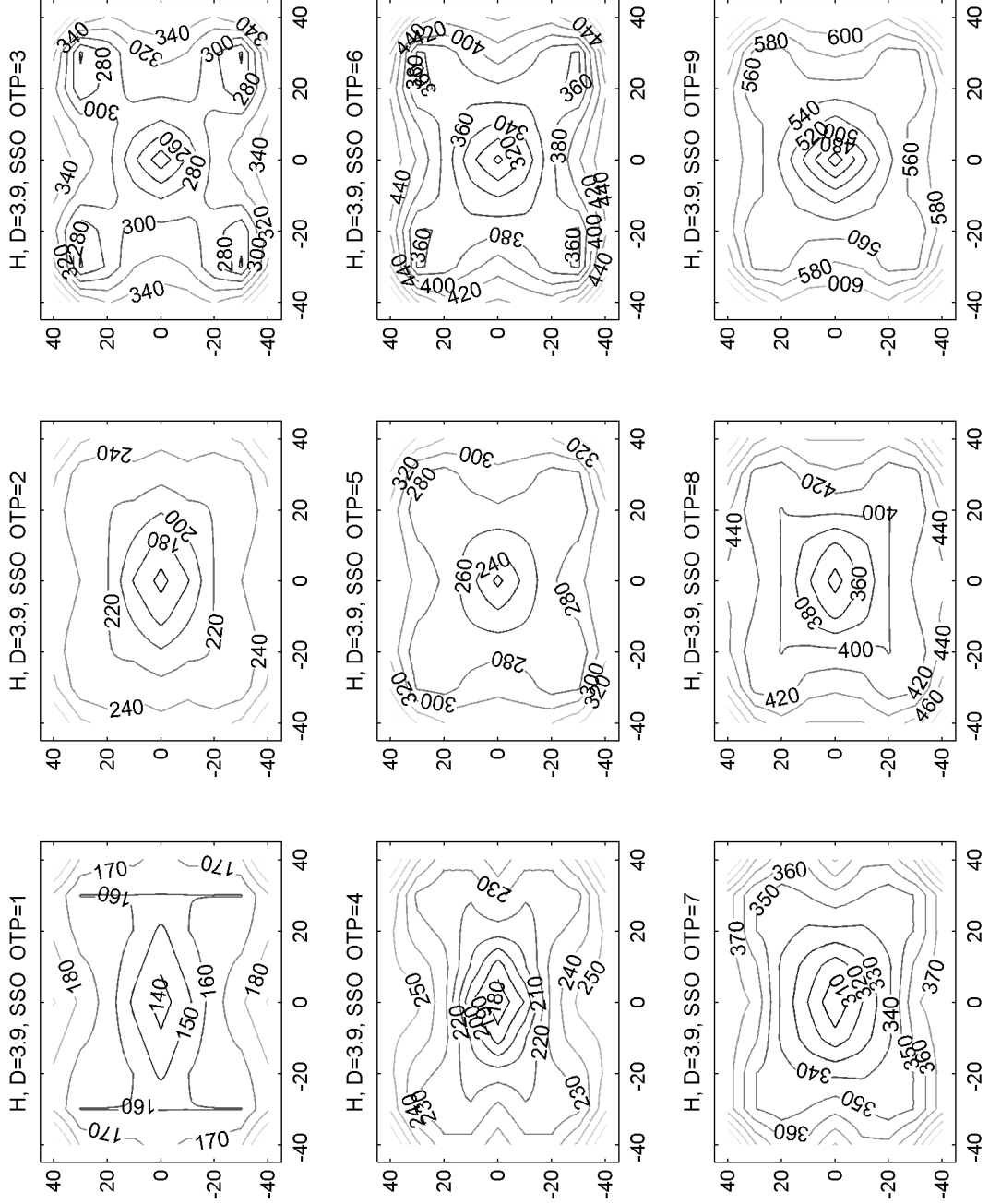


Figure 10 MCAO simulation results (using YAO) for EE50 parameter (units of milli-arcseconds) at H-Band wavelengths for the AAO 3.9m telescope with the SSO Model-OTP (1-9). The x and y axis of the contour plots denote angular field of view (units of arcseconds).

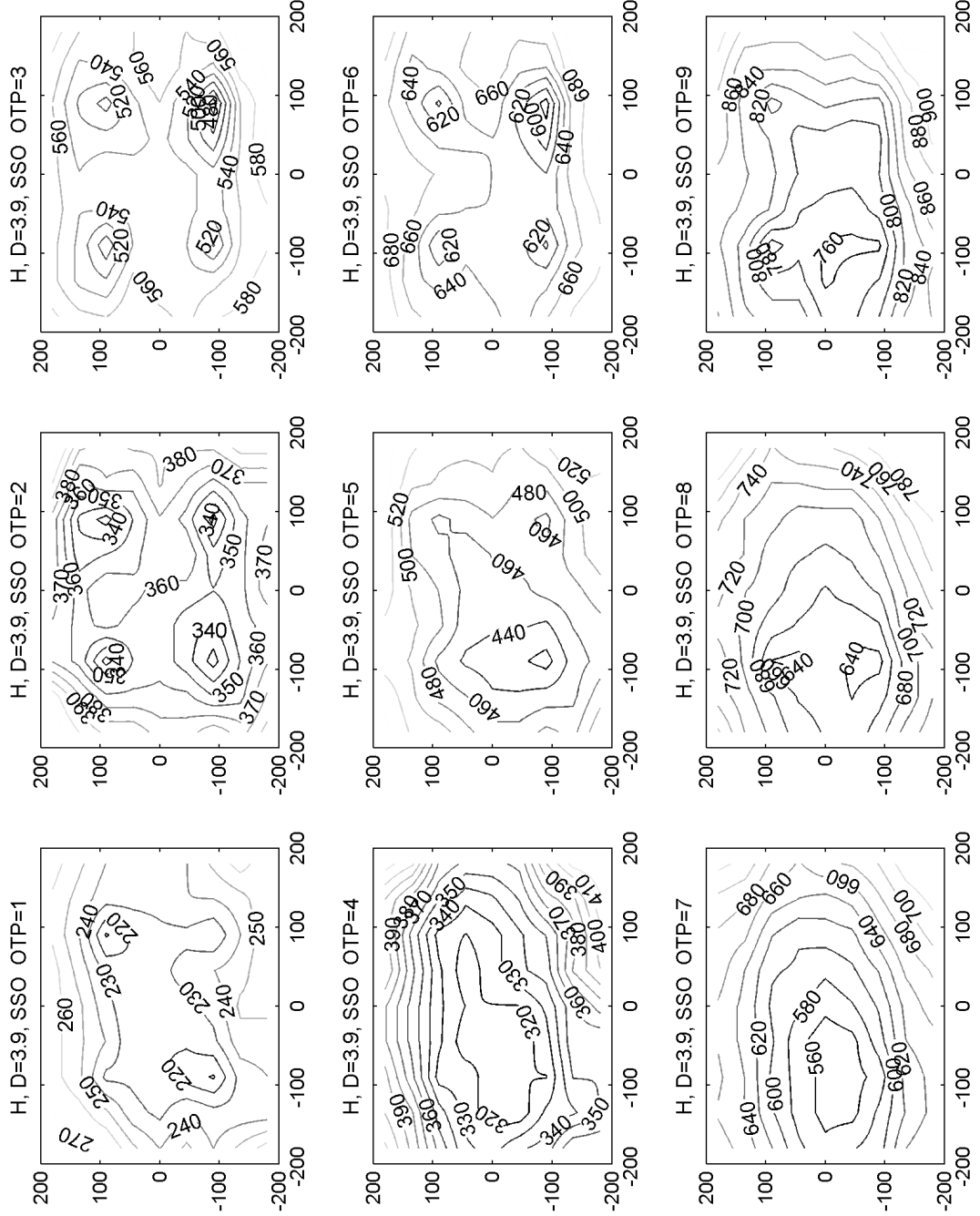


Figure 11 GLAO simulation results (using YAO) for EE50 parameter (units of milli-arcseconds) at H-Band wavelengths for the AAO 3.9m telescope with the SSO Model-OTP (1-9). The x and y axis of the contour plots denote angular field of view (units of arcseconds).